Chemistry–A European Journal
Research Article
doi.org/10.1002/chem.202304174
Chemistry Europe
European Chemical Societies Publishing
www.chemeurj.org

Hot Paper

Photochemical Action Plots Reveal Red-shifted Wavelength-dependent Photoproduct Distributions

Joshua A. Carroll[+],[a, b] Fred Pashley-Johnson[+],[a, b, c] Hendrik Frisch,[a, b] and Christopher Barner-Kowollik*[a, b, d]

Photochemical action plots are a powerful tool for mapping photochemical reaction outcomes wavelength-by-wavelength. Typically, they map either the depletion of a reactant or the formation of a specific product as a function of wavelength. Herein, we exploit action plots to simultaneously map the formation of several photochemical products from a single chromophore. We demonstrate that the wavelength-resolved mapping of two reaction products formed during the irradiation of a chalcone species not only shows wavelength dependence – exhibiting the typical strong red-shift of the photochemical reactivity compared to the absorbance spectrum of the chromophore – but also a strong wavelength selectivity with remarkably different product distributions resulting from different irradiation wavelengths.

Introduction

The field of photochemistry is on the verge of undergoing a precision transformation. Whilst photochemical reactions have previously routinely been induced by broadly emitting light sources, the use of narrowly emitting LEDs and monochromatic laser systems has enabled access to synergistic,[1] orthogonal,[2] cooperative,[3] and antagonistic[4] reaction modes that have previously been inaccessible. The basis for accessing such reaction modes is the deep understanding of the effectiveness and outcomes of photochemical reactions at individual (monochromatic) wavelengths, which can be obtained via wavelength-resolved photochemical action plots.[5] During an action plot measurement, identical aliquots of a reaction solution are irradiated with an identical number of photons of a given wavelength and an analytical technique is employed – for example NMR spectroscopy – to map either the depletion of the starting materials or the formation of a specific product. By now, there are countless examples of recorded action plots[6] and the vast majority of these have shown a pronounced mismatch between the wavelength resolved reactivity and the extinction spectrum of the chromophore in question – a phenomenon that our team identified[7] and that is now acknowledged by many other research teams.[8] The origin of the fundamental mismatch between photochemical reactivity and absorptivity is still unknown, although we recently proposed a set of hypotheses, which await experimental testing.[5b]

Wavelength-gated processes operate under two distinct regimes: wavelength selectivity, whereby the outcome of a reaction is different at varying wavelengths, and wavelength dependence, where the efficiency of the reaction is wavelength-mediated, but the outcome is the same regardless.[9] When considering wavelength-dependent reactions of a single chromophore, product distributions are generally expected to be equivalent and match the absorption spectrum as a consequence of rapid intramolecular vibrational relaxation to the lowest excited state,[10] where most reactions are likely to occur from.[11] For example, our group has previously studied the photoproduct distributions of styrylpyrene's dimerisation and found that despite the strong red-shifted reactivity compared to the extinction spectrum, all isomers of the dimer had approximately the same action plot shape and therefore photoproduct distributions.[12] However, some cases have been documented where reactions from a single chromophore have resulted in varied pathways and product formation rates based on different irradiation wavelengths – thus exhibiting wavelength selectivity.[13] These studies have evidenced that irradiation in specific regions of the extinction spectrum are able to result in specific product formation, yet have never been assessed into the regions of extremely low absorptivity. Critically, in some cases the methods of determination of

[a] J. A. Carroll,[+] F. Pashley-Johnson,[+] Prof. H. Frisch, Prof. C. Barner-Kowollik
School of Chemistry and Physics
Queensland University of Technology (QUT)
2 George Street, Brisbane, QLD 4000, Australia
E-mail: christopher.barnerkowollik@qut.edu.au

[b] J. A. Carroll,[+] F. Pashley-Johnson,[+] Prof. H. Frisch, Prof. C. Barner-Kowollik
Centre for Materials Science
Queensland University of Technology (QUT)
2 George Street, Brisbane, QLD 4000, Australia

[c] F. Pashley-Johnson[+]
Department of Organic and Macromolecular Chemistry, Polymer Chemistry Research Group, Centre of Macromolecular Chemistry (CMaC), Faculty of Science,
Ghent University, Krijgslaan 281 (S4-Bis), 9000 Ghent, Belgium

[d] Prof. C. Barner-Kowollik
Insitute of Nanotechnology (INT)
Karlsruhe Institute of Technology (KIT), Hermann-von-Helmholtz-Platz 1, 76344 Eggenstein-Leopoldshafen, Germany

[+] J.A.C and F.P.-J contributed equally to this work

Supporting information for this article is available on the WWW under https://doi.org/10.1002/chem.202304174

quantum yield at each wavelength are indirect and lack the wavelength resolution available from tuneable laser systems.

Herein, we demonstrate through an in-depth photochemical action plot analysis that it is possible to directly access individual product yields from a single chromophore as a function of irradiation wavelength. Importantly, we reveal product formation maxima at odds with the extinction spectra in regions of extremely low absorptivity and show very high selectivity over reaction outcomes. We explore pyrene-chalcone (**PyChal**, Scheme 1) as our model chromophore.[6b,14] The chromophore has two principle reaction modes upon irradiation with light: either a [2+2] photocycloaddition, or cis/trans isomerisation around the central double bond. Here, we map the depletion of the starting isomer (***trans*-PyChal**) and in parallel the formation of the cycloadduct (**(PyChal)$_2$**) and the isomerisation product (***cis*-PyChal**) as a function of monochromatic irradiation wavelength. We note – given previous findings from photochemical action plots – that there is no a priori expectation as to how much of each product is generated at each specific wavelength and how red-shifted each product formation will be.

Results and Discussion

Initially, we assign the structures of each of the species using high-performance liquid chromatography coupled to electrospray ionisation high-resolution mass spectrometry (HPLC-ESI-HRMS) and ^{1}H NMR. Figure 1b shows the HPLC-ESI-HRMS chromatographs for the monomer solution and two extremes of the product formation. We observe that upon irradiation with 470 nm light, a more polar species arises at shorter retention time with *m/z* 479.1845, corresponding to the undimerized **PyChal** ([**PyChal**+H]+ *m/z* calcd.=479.1849; supporting information section 12). In the ^{1}H NMR spectrum for the same irradiation wavelength (Figure 1c, middle), we observe the double-bond associated resonance of ***trans*-PyChal** at 9.25 ppm depleting, whilst a new double bond resonance appears at 6.71 ppm with a *J* coupling value of 12.5 Hz, shifted by 15.3 Hz compared to before irradiation. This decrease in the *J* coupling constant,[12] combined with the shift to earlier retention times in the HPLC trace,[15] allows us to conclude that the ***trans*-PyChal** has undergone geometric isomerisation to ***cis*-PyChal**. The second product is seen to undergo a shift to longer retention times in the HPLC trace (Figure 1b, top), which is also accompanied by a shift to higher molecular weight, with *m/z* corresponding to a dimer (*m/z* [**(PyChal)$_2$**+H]+ calcd.= 957.3633; experimental=957.3641). The ^{1}H NMR spectrum further evidences the dimerisation, with the distinctive formation of cyclobutene associated resonances at 5.81 and 5.52 ppm. Thus, the formed product is **(PyChal)$_2$**.

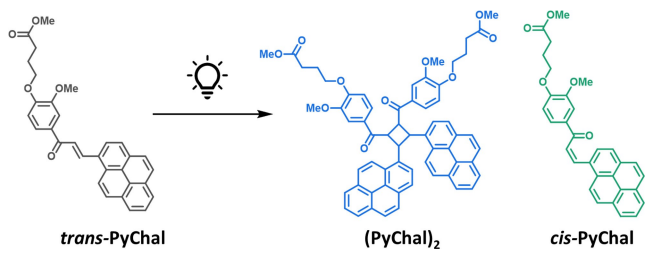

Scheme 1. The photochemical chalcone reaction manifold. Upon irradiation with visible light, ***trans*-PyChal** can undergo either dimerisation to **(PyChal)$_2$** or isomerisation to ***cis*-PyChal**.

Following the methodology employed in our previous study on the photochemical behaviour of **PyChal**,[6b] we monitored the depletion of the β-alkene proton resonance at 9.25 ppm with respect to the integral of the internal standard (1,3,5-trimethoxybenzene), allowing us to determine the starting material consumption as a function of wavelength (Figure 2a). The action plot demonstrates the typical red-shifted activity compared to the extinction spectrum (shown in purple in Figure 2a) that we have experimentally observed previously for [2+2] photocycloadditions as well as other photochemical processes.[5a] The photochemical action plot features a multimodal character with a global maximum activity at 440 nm and a smaller local maximum 20 nm red-shifted at 460 nm.

In addition to monitoring the depletion of starting material, we monitor the formation of both photoproducts. We employ the ***cis*-PyChal**'s double bond associated resonance at 6.71 ppm and the **(PyChal)$_2$**'s cyclobutane resonance at 5.81 ppm to monitor the formation of each species (resonances labelled in Figure 1c), mapping the formation of each product as a function of wavelength (Figure 2b). The formation of **(PyChal)$_2$** – whilst clearly red-shifted relative to the extinction spectrum – occurs more readily at shorter wavelengths when compared to the isomerisation, which also shows two remarkably red-shifted reactivity maxima at 445 nm and 470 nm. The [2+2] photocycloaddition is known to proceed through a triplet state due to the required orbital overlap[16] – confirmed by our finding that nearly no conversion to the dimer is observed in the presence of oxygen (Figure S23) and the ***trans*- to *cis*-**isomerisation of similar systems has also been shown to proceed via a triplet state.[17] We still observe isomerisation in the presence of oxygen (Figure S23), which we hypothesize is due to the rapid, unimolecular nature of the reaction that is not sufficiently rapidly quenched by oxygen. Thus, we postulate that upon irradiation with different wavelengths of light, different singlet energy states are populated that subsequently undergo intersystem crossing to different triplet states, which favour different photochemical outcomes.

To gain insight into the reason behind the disparate product distributions with different wavelengths, we probed the fluorescence excitation spectra of the ground state ***trans*-PyChal** molecule at thew lower concentration of 1 μM (Figure S17). It is important to note the distinction that extinction spectra (commonly conflated with absorption spectra) measure the amount of light absorbed and scattered by a sample by linear irradiation/detection, whereas excitation spectra monitor the photoluminescent (PL) emission intensity at a given wavelength perpendicular to the path of the excitation light source. We noticed that two distinct excitation profiles exist, responsible for the shorter and longer wavelength emissions (shown in Figure 3 for the emission at 460 nm and 580 nm in blue and

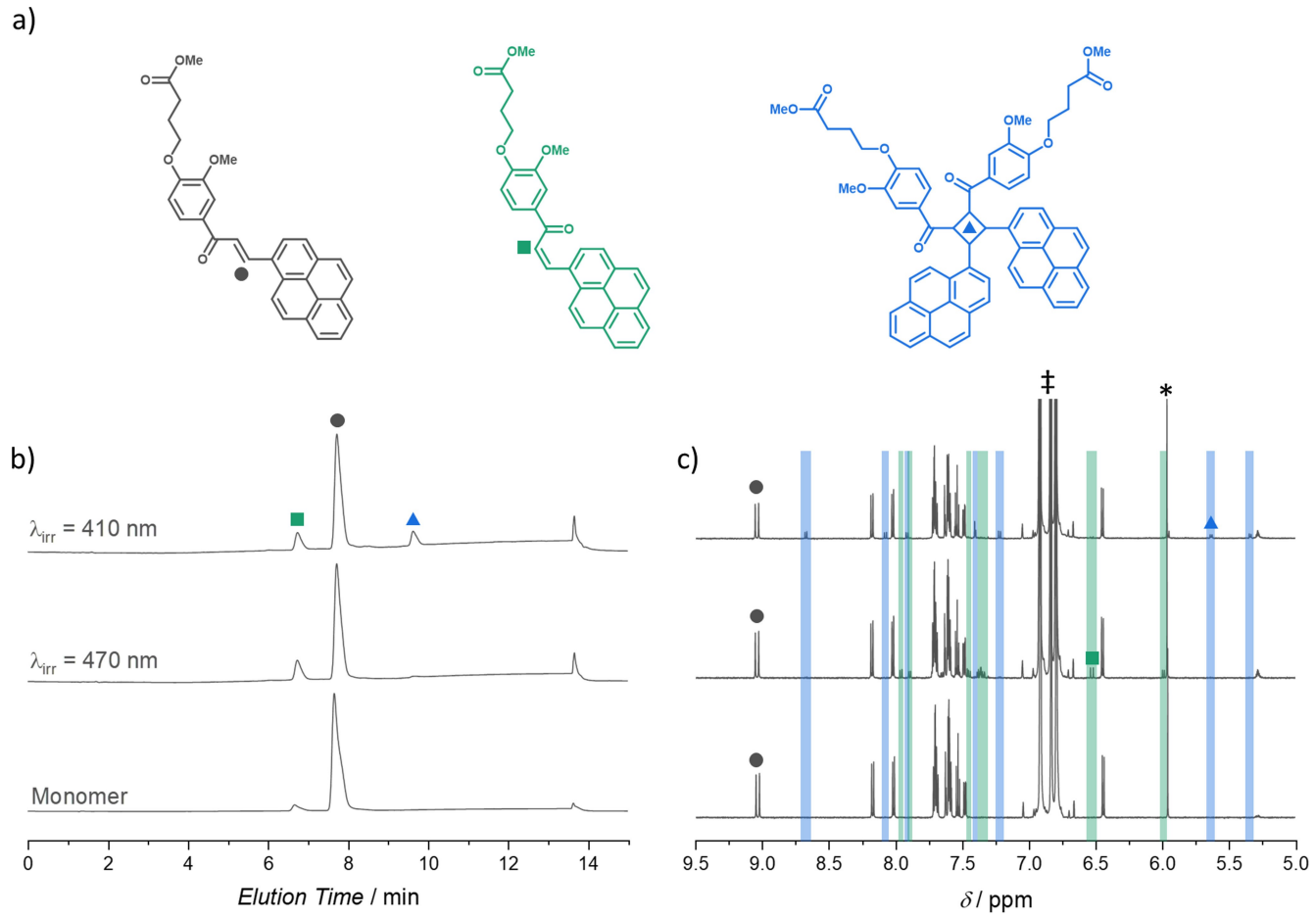

Figure 1. (a) Structures of ***trans*-PyChal**, ***cis*-PyChal**, and **(PyChal)$_2$** (only one isomer shown), with a dot indicating the proton resonances that were integrated to determine the concentration of each species. (b) HPLC-ESI-HRMS chromatographs showing the monomer solution before irradiation (bottom), the solution after irradiation with 470 nm light (middle) and after irradiation with 410 nm light (top) coloured dots show the peaks that correspond to each species based on the *m/z* of the base peak in the mass spectrum (refer to the Supporting Information section 12.1 and 12.2 for the mass spectra). (c) ^{1}H NMR spectra of the monomer solution before irradiation (bottom), after irradiation with 470 nm light (middle) and after irradiation with 410 nm light (top) – coloured dots indicate the protons resonances that are integrated to monitor conversion, corresponding to the protons labelled in Figure 1a; highlighted sections show resonances that are unique to each of the species. ‡ shows solvent resonances from d_8-toluene and * is the -OCH$_3$ resonance of the internal standard, 1,3,5-trimethoxy benzene. All samples were monochromatically irradiated at the given wavelength with 9 μmol of photons over 5 minutes at a concentration of 1 mM in d8-toluene (500 μL).

green respectively). Interestingly, the fluorescence emission spectra at varied concentrations show a similar change, whilst only the 1 μM concentration reveals the two distinct excitation profiles. When the ratio of **(PyChal)$_2$** formation to ***cis*-PyChal** formation is overlaid with these excitation spectra, we notice a clear correlation between the products formed and the prevalence of each profile in the excitation spectra. For 410 to 440 nm, the blue-shifted excitation profile is the major feature in the excitation spectrum, where a much higher prevalence of the **(PyChal)$_2$** formation is observed. The only other wavelength where the ratio of **(PyChal)$_2$** to ***cis*-PyChal** formation is again above unity is at 460 nm, where a local minimum is observed in the red-shifted excitation profile. The photodiode array from the HPLC-ESI-HRMS shows that the isolated products each absorb at shorter wavelengths than **PyChal** (Figure S14), ruling their contributions to the red-shifted excitation spectrum out. In addition, extinction spectra acquired at concentrations of 1 μM, 10 μM and 1 mM show identical molar extinction between 450 nm and 500 nm (Figure S15), suggesting that there is very little absorption in this region.

The possibility for any aggregation phenomena contributing to the observed effects was explored, and extinction spectra of the **PyChal** monomer in toluene with increasing fractions of cyclohexane (a poor solvent for **PyChal**) were collected (Figure S21). No visible splitting due to aggregation was observed, and the extinction spectrum at high fractions of cyclohexane to toluene shifted to match the extinction spectrum observed in pure cyclohexane. The spectra follow a linear decrease in maximum extinction with increasing cyclohexane volume fraction. The fluorescence emission at varying concentrations was also studied (Figure S22), and outside of some self-absorption there was a linear relationship observed between concentration and emission intensity (Figure S23), implying an absence of aggregation induced emission. It is possible that a weak symmetry forbidden $S_0 \rightarrow S_1$ transition exists at these longer wavelengths, as has been shown previously for similar

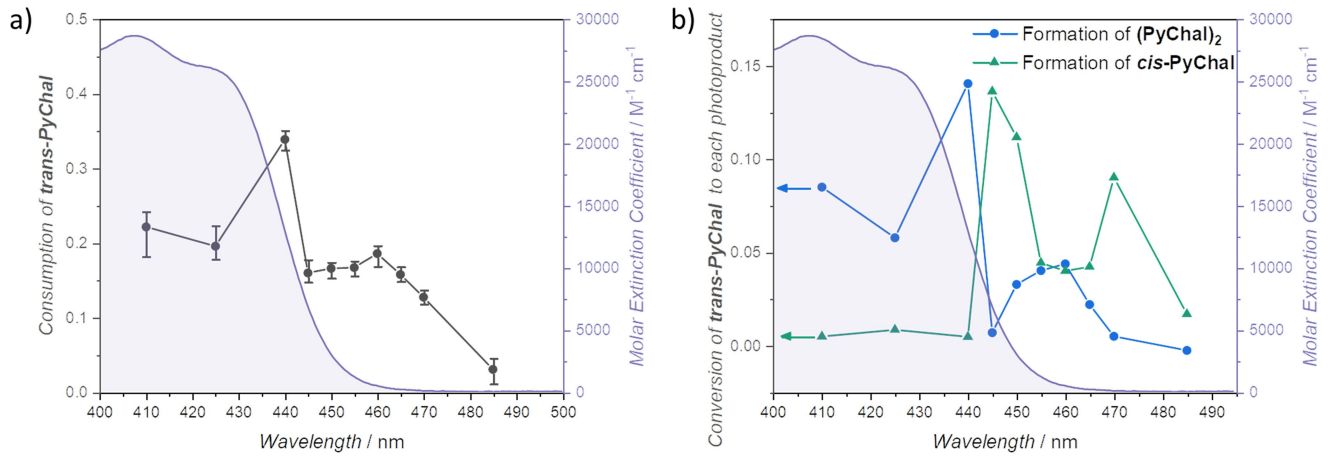

Figure 2. (a) Photochemical action plot showing the depletion of ***trans*-PyChal** as a function of wavelength. The consumption of ***trans*-PyChal** determined by the depletion of the β-alkene proton's ^{1}H NMR resonance is shown in grey, whilst the molar extinction spectrum at the concentration of 10 μM is shown in purple. (b) Photochemical action plot showing the formation of the two products ***cis*-PyChal** (green) and **(PyChal)$_2$** (blue) as determined by the population of the α-alkene proton and cyclobutane proton's ^{1}H NMR resonances respectively, with the extinction spectrum shown in purple. All samples were irradiated at the given monochromatic wavelength with 9 μmol of photons over 5 minutes at the concentration of 1 mM in d_8-toluene (500 μL). Each wavelength-resolved experiment was repeated in triplicate, the data point shows the mean value. Refer to the Supporting Information section 6 for the associated error. Conversion and consumption values are given as a fraction where 1 indicates complete conversion/consumption.

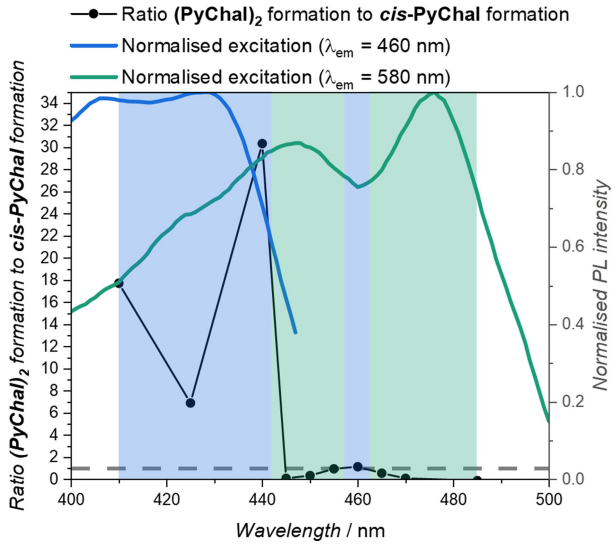

Figure 3. Ratio of **(PyChal)$_2$** formation to ***cis*-PyChal** formation as a function of wavelength (black circles) overlaid with the excitation spectrum of ***trans*-PyChal** at 460 nm (blue) and 580 nm (green). The excitation spectra were recorded at a concentration of 1 μM in toluene and are smoothed with a moving mean of ±3.5 nm. The grey dotted line maps the ratio of **(PyChal)$_2$** formation to ***cis*-PyChal** formation = 1, below which more ***cis*-PyChal** is formed, and above which more **(PyChal)$_2$** is formed.

pyrene derivatives,[18] suggesting that at shorter wavelengths we may preferentially excite symmetry-allowed $S_0 \rightarrow S_2$ or $S_0 \rightarrow S_3$ transitions that are visible in the excitation spectrum, leading to lower rates of vibrational relaxation to S_1. However, when irradiating with much longer wavelengths (>460 nm), the symmetry-forbidden transition becomes the most prevalent, leading to intersystem crossing (ISC) to different triplet states with potentially different photochemical outcomes. Whilst this transition would be rare in comparison to excitation to higher orbitals, it may provide much more efficient access to molecular geometries and ISC rates than achievable from higher orbitals. We note that wavelength-dependent time-resolved spectroscopy would be required to explore the matter in detail. Different ground state conformations of the ***trans*-PyChal** molecule may also allow for the observed wavelength selectivity, where variations in localised solvent environments allow for selective excitation at longer wavelengths of specific conformations.[19] These effects can be especially impactful on isomerisation rates where differing solvent environments affect the energy of the molecule, and red-edge effects are present.[20]

Conclusions

We herein demonstrate for the first time that photochemical action plots can be used to reveal remarkably different photochemical outcomes from a single chromophore, simply as a function of wavelength. Photochemical action plots have previously been shown to be of immense value due to their ability to reveal the otherwise unpredictable wavelength of maximum reactivity for given chromophores. Our current work demonstrates the value of and necessity for photochemical action plots to quantify and selectively target reaction outcomes, as well as to maximise the yield of a given photoproduct.

Acknowledgements

C.B.-K. acknowledges funding by the Australian Research Council (ARC) in the form of a Laureate Fellowship enabling his photochemical research program. H.F. is grateful for a DECRA Fellowship from the ARC. C.B.-K. and H.F. acknowledge continuous support by QUT's Centre for Materials Science. All authors acknowledge QUT's Central Analytical Research Facility (CARF)

supported by QUT's Research Portfolio F.P.-J. acknowledges QUT for a PhD scholarship. All the authors thank Mr. Bailey Richardson (QUT) for helpful discussions throughout the project. Open Access publishing facilitated by Queensland University of Technology, as part of the Wiley - Queensland University of Technology agreement via the Council of Australian University Librarians.

Conflict of Interests

The authors declare no conflict of interest.

Data Availability Statement

The data that support the findings of this study are available from the corresponding author upon reasonable request.

Keywords: photochemistry · action plot · wavelength-selectivity · photocyclizations · photoisomerization

[1] a) M. Regehly, Y. Garmshausen, M. Reuter, N. F. Konig, E. Israel, D. P. Kelly, C. Y. Chou, K. Koch, B. Asfari, S. Hecht, *Nature* **2020**, *588*, 620–624; b) V. Hahn, P. Rietz, F. Hermann, P. Müller, C. Barner-Kowollik, T. Schlöder, W. Wenzel, E. Blasco, M. Wegener, *Nat. Photonics* **2022**, *16*, 784–791.
[2] a) E. Rossegger, J. Strasser, R. Holler, M. Fleisch, M. Berer, S. Schlogl, *Macromol. Rapid Commun.* **2023**, *44*, e2200586; b) Y. Venkatesh, A. Chaudhuri, S. Mondal, S. S. Shah, N. D. P. Singh, *Org. Lett.* **2020**, *22*, 295–299; c) M. M. Lerch, M. J. Hansen, W. A. Velema, W. Szymanski, B. L. Feringa, *Nat. Commun.* **2016**, *7*, 12054; d) C. Dertnig, G. Guedes de la Cruz, D. Neshchadin, S. Schlögl, T. Griesser, *Angew. Chem. Int. Ed.* **2022**, *135*, e202215525.
[3] T. N. Eren, F. Feist, K. Ehrmann, C. Barner-Kowollik, *Angew. Chem. Int. Ed.* **2023**, *62*, e202307535.
[4] M. P. de Beer, H. L. van der Laan, M. A. Cole, R. J. Whelan, M. A. Burns, T. F. Scott, *Sci. Adv.* **2019**, *5*, eaau8723.
[5] a) I. M. Irshadeen, S. L. Walden, M. Wegener, V. X. Truong, H. Frisch, J. P. Blinco, C. Barner-Kowollik, *J. Am. Chem. Soc.* **2021**, *143*, 21113–21126; b) S. L. Walden, J. A. Carroll, A. N. Unterreiner, C. Barner-Kowollik, *Adv. Sci.* **2023**, *11*, e2306014.
[6] a) K. Kalayci, H. Frisch, V. X. Truong, C. Barner-Kowollik, *Nat. Commun.* **2020**, *11*, 4193; b) I. M. Irshadeen, K. De Bruycker, A. S. Micallef, S. L. Walden, H. Frisch, C. Barner-Kowollik, *Polym. Chem.* **2021**, *12*, 4903–4909; c) S. C. Gauci, F. E. Du Prez, J. O. Holloway, H. A. Houck, C. Barner-Kowollik, *Angew. Chem. Int. Ed.* **2023**, *62*, e202310274; d) M. Nardi, E. Blasco, C. Barner-Kowollik, *J. Am. Chem. Soc.* **2022**, *144*, 1094–1098.
[7] D. E. Fast, A. Lauer, J. P. Menzel, A. M. Kelterer, G. Gescheidt, C. Barner-Kowollik, *Macromolecules* **2017**, *50*, 1815–1823.
[8] a) Q. Ti, L. Fang, W. Zhao, L. Bai, H. Zhao, X. Ba, W. Chen, *J. Am. Chem. Soc.* **2023**, *145*, 26160–26168; b) C. Ma, T. Han, S. Efstathiou, A. Marathianos, H. A. Houck, D. M. Haddleton, *Macromolecules* **2022**, *55*, 9908–9917; c) I. Bakanas, J. C. Tang, R. Sarpong, *Chem. Commun.* **2023**, *59*, 3858–3861.
[9] S. Protti, D. Ravelli, M. Fagnoni, *Photochem. Photobiol. Sci.* **2019**, *18*, 2094–2101.
[10] M. Kasha, *Discuss. Faraday Soc.* **1950**, *9*, 14–19.
[11] N. J. Turro, V. Ramamurthy, J. Scaiano, *Modern Molecular Photochemistry of Organic Molecules*, University Science Books, **2010**.
[12] D. E. Marschner, H. Frisch, J. T. Offenloch, B. T. Tuten, C. R. Becer, A. Walther, A. S. Goldmann, P. Tzvetkova, C. Barner-Kowollik, *Macromolecules* **2018**, *51*, 3802–3807.
[13] a) A. Bogdanova, V. V. Popik, *J. Am. Chem. Soc.* **2003**, *125*, 1456–1457; b) D. Madea, S. Mahvidi, D. Chalupa, T. Mujawar, A. Dvorak, L. Muchova, J. Janos, P. Slavicek, J. Svenda, L. Vitek, P. Klan, *J. Org. Chem.* **2020**, *85*, 13015–13028; c) H. Fidder, A. Lauer, W. Freyer, B. Koeppe, K. Heyne, *J. Phys. Chem. A* **2009**, *113*, 6289–6296.
[14] M. Van De Walle, K. De Bruycker, J. P. Blinco, C. Barner-Kowollik, *Angew. Chem. Int. Ed.* **2020**, *59*, 14143–14147.
[15] a) H. Jin, Y. Liu, Z. Guo, F. Yang, J. Wang, X. Li, X. Peng, X. Liang, *J. Agric. Food Chem.* **2015**, *63*, 500–508; b) C. Dugave, L. Demange, *Chem. Rev.* **2003**, *103*, 2475–2532.
[16] S. Poplata, A. Troster, Y. Q. Zou, T. Bach, *Chem. Rev.* **2016**, *116*, 9748–9815.
[17] D. Schulte-Frohlinde, H. Görner, *Pure Appl. Chem.* **1979**, *51*, 279–297.
[18] E. M. Espinoza, J. A. Clark, J. B. Derr, D. Bao, B. Georgieva, F. H. Quina, V. I. Vullev, *ACS Omega* **2018**, *3*, 12857–12867.
[19] M. Jozefowicz, J. R. Heldt, *J. Fluoresc.* **2011**, *21*, 239–245.
[20] A. P. Demchenko, *Luminescence* **2002**, *17*, 19–42.

Manuscript received: December 14, 2023
Accepted manuscript online: January 24, 2024
Version of record online: February 9, 2024